Dear author,

Please note that changes made in the online proofing system will be added to the article before publication but are not reflected in this PDF.

We also ask that this file not be used for submitting corrections.

Nano Energy ∎ (∎∎∎∎) ∎∎∎–∎∎∎

Contents lists available at ScienceDirect

Nano Energy

journal homepage: www.elsevier.com/locate/nanoen

Graphene-wrapped nickel sulfide nanoprisms with improved performance for Li-ion battery anodes and supercapacitors

Ayman A. AbdelHamid, Xianfeng Yang, Jinhua Yang, Xiaojun Chen, Jackie Y. Ying*

Institute of Bioengineering and Nanotechnology, 31 Biopolis Way, The Nanos, Singapore 138669, Singapore

ARTICLE INFO

Article history:
Received 23 July 2015
Received in revised form
23 May 2016
Accepted 26 May 2016

Keywords:
Li-ion battery
Supercapacitor
Nickel sulfide
Graphene
Nanoparticles
Nanoprisms

ABSTRACT

Nickel sulfide and graphene-wrapped nickel sulfide nanoprisms were synthesized using a facile one-pot method and evaluated as anode materials for Li-ion batteries, and as supercapacitor electrodes. Graphene wrapping significantly improved the performance of nickel sulfide both as Li-ion battery anode and supercapacitor electrode. As Li-ion battery anode, graphene-wrapped nickel sulfide nanoprisms achieved an excellent specific capacity of over 1200 mAh/g after 100 cycles, and showed improved rate capability. As supercapacitor electrode, nickel sulfide nanoprisms achieved a specific capacitance of over 1000 F/g at a current density of 5 A/g, which is one of the best results reported for nickel sulfide. However, specific capacitance was much lower at 10 and 20 A/g. Introducing graphene significantly improved the specific capacitance of nickel sulfide at high current densities.

1. Introduction

Energy conversion and storage are a major global challenge due to issues associated with fossil fuels, such as pollution and non-sustainability [1,2]. To tackle this problem, it is necessary to reduce fossil fuel consumption and shift to renewable and environmentally friendly energy sources. Energy storage devices are needed to store renewable energy, such as for electric vehicles, and to integrate such energy into the power grid. Li-ion batteries and supercapacitors are promising electrochemical systems for these applications [1].

A promising approach for designing high-performance energy storage materials is reducing the particle size to the nanometer scale. For Li-ion batteries, nanoparticles can induce reactions for Li^+ storage that are not allowed by bulk materials [3]. Nanomaterials also help to accommodate the strain that accompanies the charge and discharge processes, thus improving the electrode stability [4]. The nanometer grain size reduces electron and Li^+ path lengths, thus improving rate capability [5]. In addition, the large surface area of nanoparticles provides excellent contact with the electrolyte, which helps to improve the power capability of the electrode [4,5]. For pseudocapacitors, nanoparticles facilitate ionic and electronic transport [6] due to shortened diffusion lengths. They also increase surface area [7], leading to more exposed electroactive sites and higher electrolyte transport [8].

Metal sulfides have been reported as promising Li-ion battery anode candidates, based on the "conversion reaction" [9–11], $M_x^{n+}Z_y^{m-}+nxe^-+nxLi^+ \rightleftharpoons xM^0+yLi_m^+Z^{m-}$ [12]. However, they suffer from some drawbacks, such as poor kinetics, which is manifested in electrode polarization [4], dissolution of polysulfides in the electrolyte, thus reducing its conductivity, and electrode pulverization (due to volume change during cycling), which causes capacity loss [13]. In order to overcome these challenges, new synthesis methods have been used to control the size and morphology of metal sulfides. In addition, additives such as carbon coating have been employed to improve their electrochemical properties. Xu et al. [14] synthesized shape-controlled FeS nanostructures. They observed that the performance of FeS varied according to its morphology. The presence of a carbon coating had a significant effect on the electrochemical performance of FeS. Shi et al. [13] synthesized carbon-coated cobalt sulfide nanoparticles with controlled morphology. It was found that nanodandelions have much higher cycling stability and capacity, as compared to nanoparticles. Nickel sulfide has been used as electrode material in Li-ion batteries [10,15,16]. However, rapid capacity fading was observed, which was attributed to contact loss of active materials due to volume change and formation of polysulfides [15]. Recently, composites of nickel sulfide with carbonaceous materials were used to tackle these problems. Son et al. [17] observed a rapid decay of the specific capacity of nickel sulfide upon cycling, however, the incorporation of carbon with nickel sulfide could

* Corresponding author.
E-mail address: jyying@ibn.a-star.edu.sg (J.Y. Ying).

http://dx.doi.org/10.1016/j.nanoen.2016.05.046
2211-2855/

stabilize its electrochemical properties, and capacity fading was eliminated. A specific capacity of ~470 mAh/g was achieved after 500 cycles at a current density of 1 A/g. Mahmood et al. [18] have improved the electrochemical properties of nickel sulfide by synthesizing Ni_3S_4/N-doped graphene nanocomposite in a two-step hydrothermal process. A remarkable specific capacity of ~1300 mAh/g was achieved after 100 cycles, as compared to ~500 mAh/g for bare nickel sulfide nanoparticles. However, facile, one-pot controlled synthesis of nickel sulfide/carbon nanocomposites with high performance as Li-ion battery anode is still required for electrode applications.

Metal sulfides are also very promising pseudocapacitive materials [19–21]. Different phases and shapes of nickel sulfide have been reported to have good pseudocapacitive properties. NiS hollow spheres [22], NiS_2 nanocubes [23] and Ni_3S_2 nanoflakes [24] have shown specific capacitances of 927, ~350 and 664 F/g at current densities of 4.08, 5 and 4 A/g, respectively. However, electrode pulverization occurred over prolonged cycling, which led to capacity loss. One of the promising approaches for tackling this problem was to use composites of nickel sulfide with carbonaceous materials in order to stabilize their performance during cycling [25]. Wang et al. [26] reported higher capacity and cycling stability of NiS/graphene oxide (GO) nanocomposite than NiS and GO alone. Yang et al. [25] showed that the introduction of carbon nanotubes or reduced GO (RGO) to NiS improved its cycling stability significantly. It would be of interest to manipulate the phase, size and shape of nickel sulfide in order to improve its pseudocapacitive performance. This can be combined with carbon coating and graphene wrapping to enhance the electrode conductivity and improve its cycling stability.

Herein, we report a facile, one-pot and inexpensive method for the synthesis of nickel sulfide and graphene-wrapped nickel sulfide nanoprisms. They were used as Li-ion battery anodes and supercapacitor electrodes. The nickel sulfide nanoprisms allowed for good interaction with the electrolyte, short ion paths and enhanced kinetics [14]. Graphene wrapping provided a support for the dispersion of nickel sulfide nanoprisms, thus enhancing surface area and contact with the electrolyte. It also helped to buffer the volume change of nickel sulfide during insertion and extraction of Li ions, thus mitigating contact loss with the current collector [27,28]. Moreover, it improved conductivity and prevented dissolution of polysulfides [29].

2. Materials and methods

2.1. Synthesis of nickel sulfide nanoprisms (NS)

51.4 mg (0.2 mmol) of nickel (II) acetylacetonate was mixed with 5 mL of oleylamine (15.2 mmol) and 1 mL of oleic acid (3.15 mmol) in a 50-mL 3-necked flask, and stirred for 30 min in argon. The solution was heated to 100 °C, and degassed for 15 min 1 mL of dodecanethiol (4.2 mmol) was injected at 100 °C, and then the temperature was increased to 250 °C where the solution was aged for 20 min. After cooling, the solution was washed with hexane and ethanol several times. The product was finally calcined at 350 °C for 1 h in argon.

2.2. Synthesis of graphene-wrapped nickel sulfide nanoprisms (NS/G)

GO was mixed with 5 mL oleylamine, and sonicated for 2 h until full dispersion. Synthesis of graphene-wrapped nickel sulfide nanoprisms was the same as that of bare nickel sulfide nanoprisms, except that GO-oleylamine was used instead of oleylamine. NS/G materials synthesized using 5 mg, 10 mg and 20 mg of GO were specified as NS/G-5, NS/G-10 and NS/G-20, respectively.

2.3. Materials characterization

NS and NS/G were characterized using transmission electron microscopy (TEM, FEI Tecnai F20), powder X-ray diffraction (XRD, PaNalytical X'pert PRO), thermogravimetric analysis (TGA, Perkin Elmer Pyris 1 TGA), Raman spectroscopy (RENISHAW in Via Raman microscope, 785 nm laser), N_2 adsorption (Micromeritics ASAP 2020), and X-ray photoelectron spectroscopy (XPS) (VG ESCALAB 220i-XL).

2.4. Electrochemical measurements

Calcined NS and NS/G were mixed with acetylene black (Denka), vapor-grown carbon fibers (VGCFs), polyvinylidene fluoride (PVDF) at a weight ratio of 8:0.5:0.5:1, and dispersed in *N*-methyl-2-pyrrolidone (NMP) to form a slurry.

2.5. Li-ion battery anode

The slurry was coated on copper foil, dried at 80 °C overnight, and then pressed. Coin cells were assembled in an argon glove box using Li metal as the counter electrode and 1 M $LiPF_6$ in ethylene carbonate and diethyl carbonate (1:1) as the electrolyte. Galvanostatic charge-discharge measurements (0.01–3 V) were conducted with Arbin BT-2000 at various current densities. Cyclic voltammetry (CV) was performed using AUTOLAB at 0.01–3 V with a scan rate of 0.5 mV/s. Electrochemical impedance spectroscopy (EIS) was conducted using AUTOLAB in the range of 100 kHz to 10 mHz. Specific capacity of NS/G was calculated based on the total mass of the nanocomposite.

2.6. Li-ion battery full cell

Full cell was assembled using $LiCoO_2$ as cathode. $LiCoO_2$, acetylene black (Denka) and PVDF with a weight ratio of 9:0.5:0.5 were used for electrode preparation. The electrode preparation process was similar to that of calcined NS. Galvanostatic charge-discharge measurements of the full cell were conducted between 0.5 V and 4.2 V. The weight ratio of the active materials in cathode and anode was controlled in order to match the capacities of both electrodes. A cathode: anode active material ratio of 13.8 was used. The specific capacity of the full cell was based on the total mass of the anode and cathode active materials.

2.7. Supercapacitor electrode

The slurry was coated on a piece of Ni foam (1 cm × 1 cm), dried at 80 °C overnight, and then pressed. Electrochemical measurements were performed in a three-electrode system in 2 M KOH electrolyte, using Pt and Ag/AgCl as counter and reference electrodes, respectively. CV was conducted using AUTOLAB at voltage scan rates of 2, 5, 10, 20 and 50 mV/s. Galvanostatic charge-discharge was performed using AUTOLAB at current densities of 3, 5, 10 and 20 A/g. The specific capacitance was calculated according to the following equation [25]:

$$C = I \times \Delta t / m \times \Delta V \quad (1)$$

where C (F/g) is the specific capacitance, I (A) is the current intensity, Δt (s) is the discharge time, m (g) is the mass of active materials, and ΔV (V) is the potential window.

3. Results and discussion

Fig. 1a shows a TEM image of bare nickel sulfide nanoparticles. The nanoparticles have a nanoprismatic shape, with the bases and

Please cite this article as: A.A. AbdelHamid, et al., Graphene-wrapped nickel sulfide nanoprisms with improved performance for Li-ion battery anodes and supercapacitors, Nano Energy (2016), http://dx.doi.org/10.1016/j.nanoen.2016.05.046

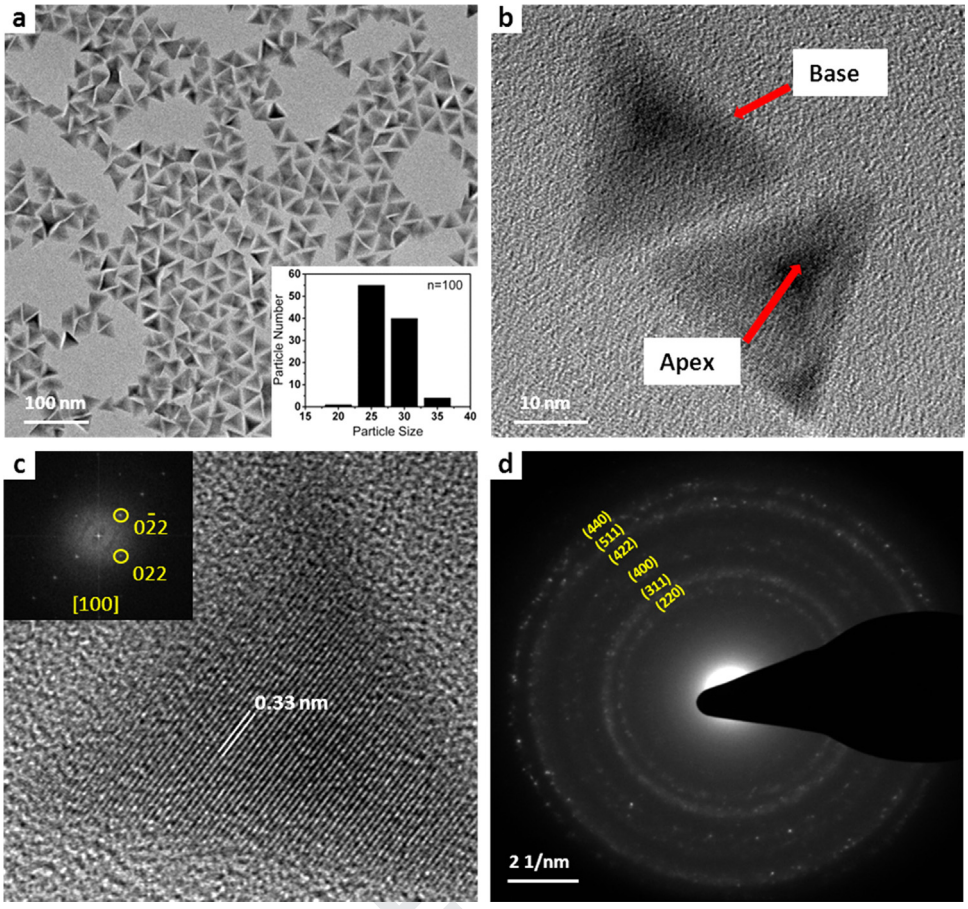

Fig. 1. (a,b) TEM images (inset in (a): particle size distribution), (c) HRTEM image (inset: corresponding FFT pattern), and (d) SAED pattern of as prepared nickel sulfide nanoprisms.

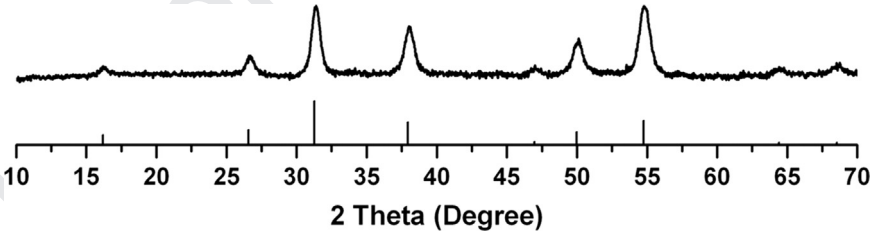

Fig. 2. XRD pattern of as-prepared nickel sulfide nanoprisms. The vertical lines correspond to Ni_3S_4 (JCPDS card #00-047-1739).

apices clearly observed in Fig. 1b. The average size of the nanoprisms was ~25 nm (Fig. 1a: inset). High-resolution TEM (HRTEM) showed that the nanoprisms were single crystals (Fig. 1c). A d-spacing of 0.33 nm was measured, which could be indexed to the (220) plane of Ni_3S_4 (JCPDS card # 00–047-1739). The single crystalline nature of the nanoprisms was confirmed by fast Fourier-transform (FFT) pattern (Fig. 1c: inset), which showed a typical pattern for single crystals [30]. Zone axis was determined to be [100]. Selected area electron diffraction (SAED) of nanoprisms showed a polycrystalline pattern (Fig. 1d). The d-spacings detected were 0.32, 0.28, 0.23, 0.21, 0.18 and 0.16 nm, which matched the (220), (311), (400), (422), (511) and (440) planes of Ni_3S_4 (JCPDS card #00-047-1739), respectively.

Fig. 2 shows the XRD pattern of nickel sulfide nanoprisms. The XRD peaks could be assigned to the cubic polydymite phase (Ni_3S_4) of space group Fd-3m (JCPDS card #00–047-1739). The peaks at $2\theta = 16.2°$, 26.7°, 31.4°, 38.01°, 47.0°, 50.1°, 54.8°, 64.4° and 68.5° could be indexed to (111), (220), (311), (400), (422), (511), (440), (533) and (444) reflections, respectively. No other peaks were observed, illustrating the phase purity of this material.

Nickel sulfide with nanoprismatic shape was previously reported using other methods, either mixed with other shapes [31,32] or alone [33]. Although the latter method could produce pure nickel sulfide nanoprisms, it required pre-synthesis of an organic precursor, which added another step to the synthesis process.

Fig. 3a and b shows the scanning transmission electron microscopy (STEM) images of NS/G-10. When nickel sulfide nanoprisms grew on the surface of GO sheets, they retained their size and nanoprismatic morphology. Their XRD peaks (Fig. 3c) were indexed to Ni_3S_4 (JCPDS card #00-047-1739), indicating that the incorporation of GO in the synthesis of nickel sulfide did not affect the morphology or phase of the nanoparticles. This was an advantage since it provided for the facile one-pot synthesis of NS/G nanocomposite. Two extra peaks were noted at $2\theta = 11.3°$ and 22.5°, which corresponded to non-reduced and reduced GO,

Please cite this article as: A.A. AbdelHamid, et al., Graphene-wrapped nickel sulfide nanoprisms with improved performance for Li-ion battery anodes and supercapacitors, Nano Energy (2016), http://dx.doi.org/10.1016/j.nanoen.2016.05.046

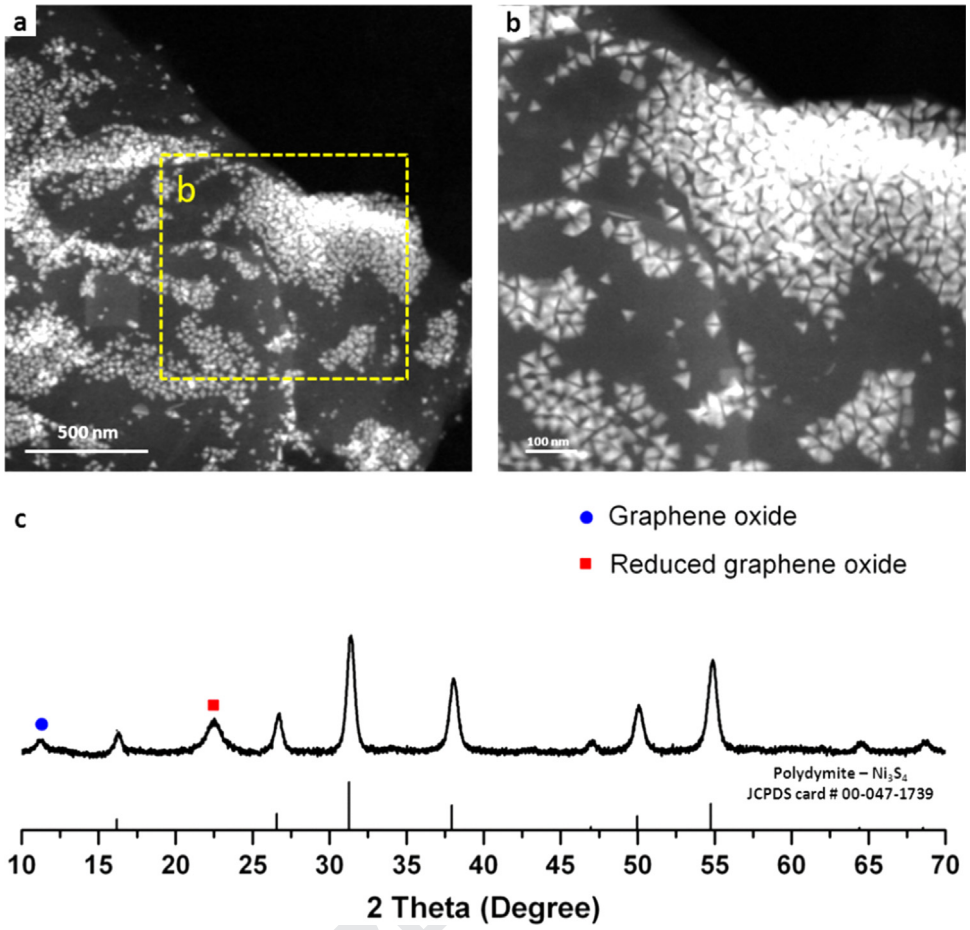

Fig. 3. (a) STEM image and (b) magnified STEM image of the boxed area in (a), and (c) XRD pattern of as-prepared NS/G-10 nanocomposite.

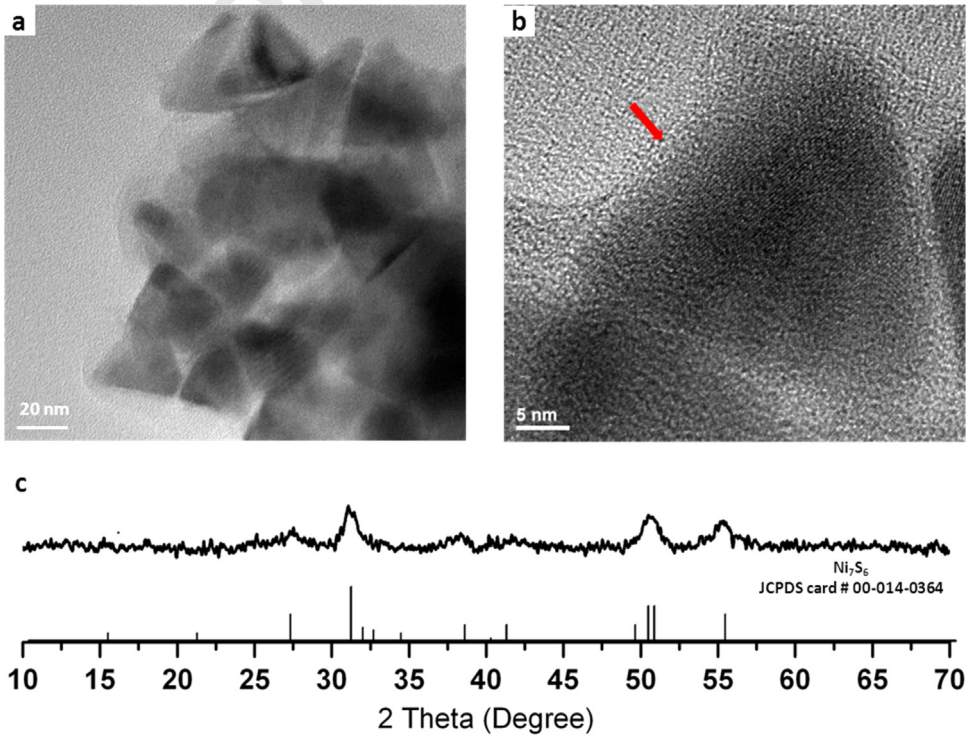

Fig. 4. (a) TEM image, (b) HRTEM image (red arrow points to the carbon layer), and (c) XRD pattern of the calcined nickel sulfide nanoprisms. (For interpretation of the references to color in this figure legend, the reader is referred to the web version of this article).

Please cite this article as: A.A. AbdelHamid, et al., Graphene-wrapped nickel sulfide nanoprisms with improved performance for Li-ion battery anodes and supercapacitors, Nano Energy (2016), http://dx.doi.org/10.1016/j.nanoen.2016.05.046

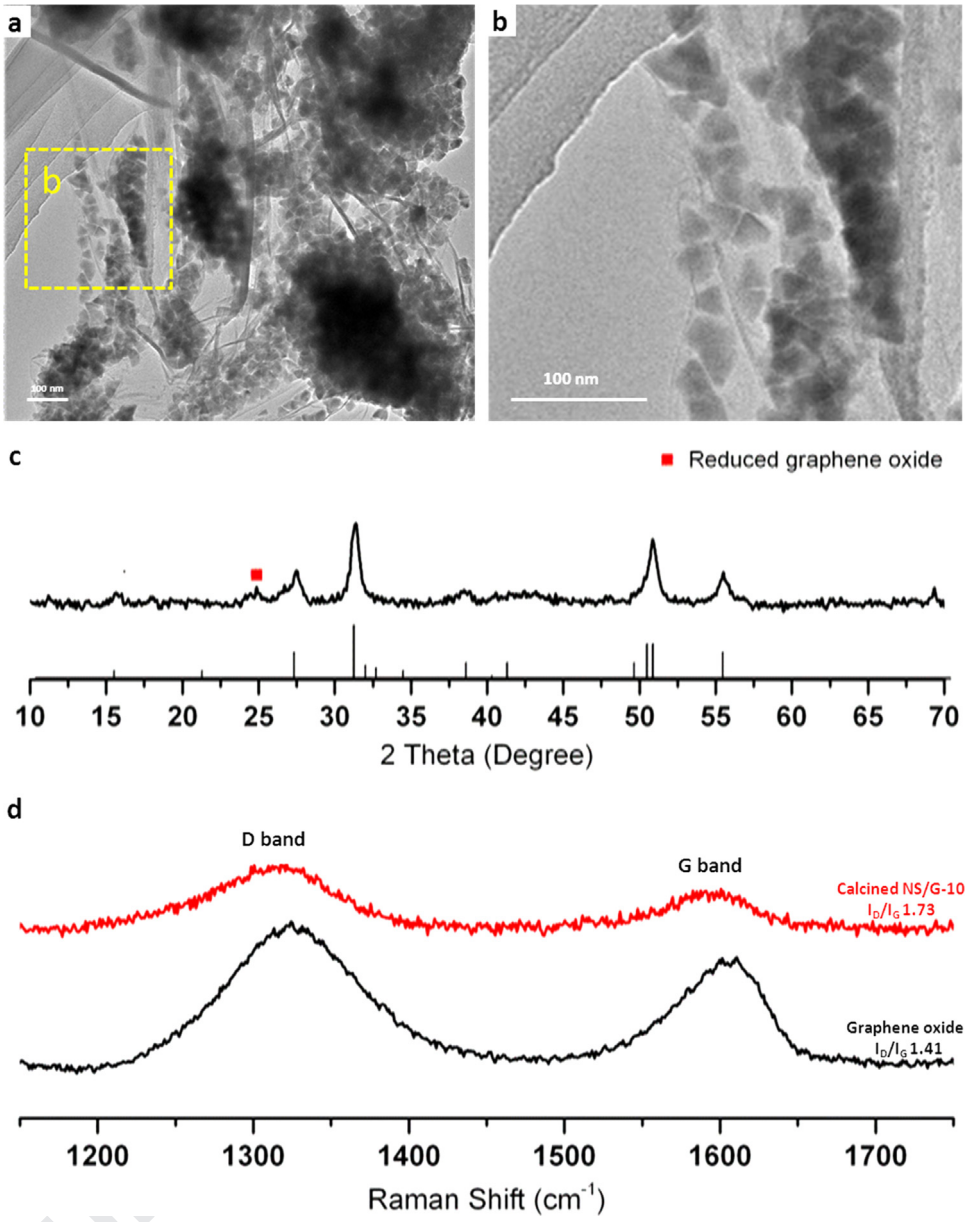

Fig. 5. (a) TEM image and (b) magnified TEM image of the boxed area in (a), and (c) XRD pattern of calcined NS/G-10. (d) Raman spectra of GO and calcined NS/G-10.

respectively [34].

Calcination was performed to carbonize the organic compounds in the samples to enhance conductivity, and to further reduce GO. The calcination temperature was chosen according to the TGA results of the synthesis precursors mixture (oleylamine: oleic acid: dodecanethiol volume ratio=5:1:1). Calcination at 350 °C for 1 h in an inert atmosphere was sufficient to decompose almost all the precursors (Fig. S1). These conditions were used to calcine the as-prepared nickel sulfide and NS/G samples.

After calcination, the bare nickel sulfide nanoprisms were aggregated, but the nanoprismatic shape remained intact (Fig. 4a). The particles were surrounded by ~4 nm-thick carbon layers due to decomposition of the capping agents (Fig. 4b). The XRD peak positions of the calcined nickel sulfide (Fig. 4c) changed slightly to 27.5°, 31.1°, 38.3°, 40.2°, 41.6°, 50.5° and 55.4°, which could be indexed to the Ni_7S_6 phase (JCPDS card #00-014-0364). This phase change could be attributed to the loss of some sulfur during calcination [18,35].

In the calcined NS/G, nickel sulfide nanoprisms were found to be well-dispersed on the surface of the graphene sheets, with no significant change in morphology (Fig. 5a and b). The nanoprisms were wrapped by graphene sheets upon calcination, which could help to improve their electrochemical properties. XRD pattern of calcined NS/G-10 showed that phase change to Ni_7S_6 had occurred (Fig. 5c). The diffraction peak of non-reduced GO at $2\theta=11.3°$ disappeared, showing further reduction of graphene oxide. The (002) peak of RGO shifted from $2\theta=22.5°$ in NS/G-10 to $2\theta=24.9°$ in calcined NS/G-10. This corresponded to a decrease of interlayer spacing from 0.395 nm to 0.358 nm, which could be due to further removal of the remaining oxygenated groups, which reduced the interlayer spacing [34].

Raman spectrum of the NS/G-10 nanocomposite (Fig. 5d) showed a G band at ~1595 cm^{-1}, assigned to the vibration of sp^2 carbon atoms in 2D lattice, and a D band at ~1317 cm^{-1} assigned to the defects in graphene layers [36]. The intensity of D band to G band (I_D/I_G) is a measure of disorder and defects, and also graphitization of the sample [36]. It was found that the I_D/I_G ratio increased from 1.41 in GO to 1.73 in NS/G-10, which could be due to the reduction of GO that generated defects. Although new sp^2 domains were restored upon GO reduction, they became smaller

Please cite this article as: A.A. AbdelHamid, et al., Graphene-wrapped nickel sulfide nanoprisms with improved performance for Li-ion battery anodes and supercapacitors, Nano Energy (2016), http://dx.doi.org/10.1016/j.nanoen.2016.05.046

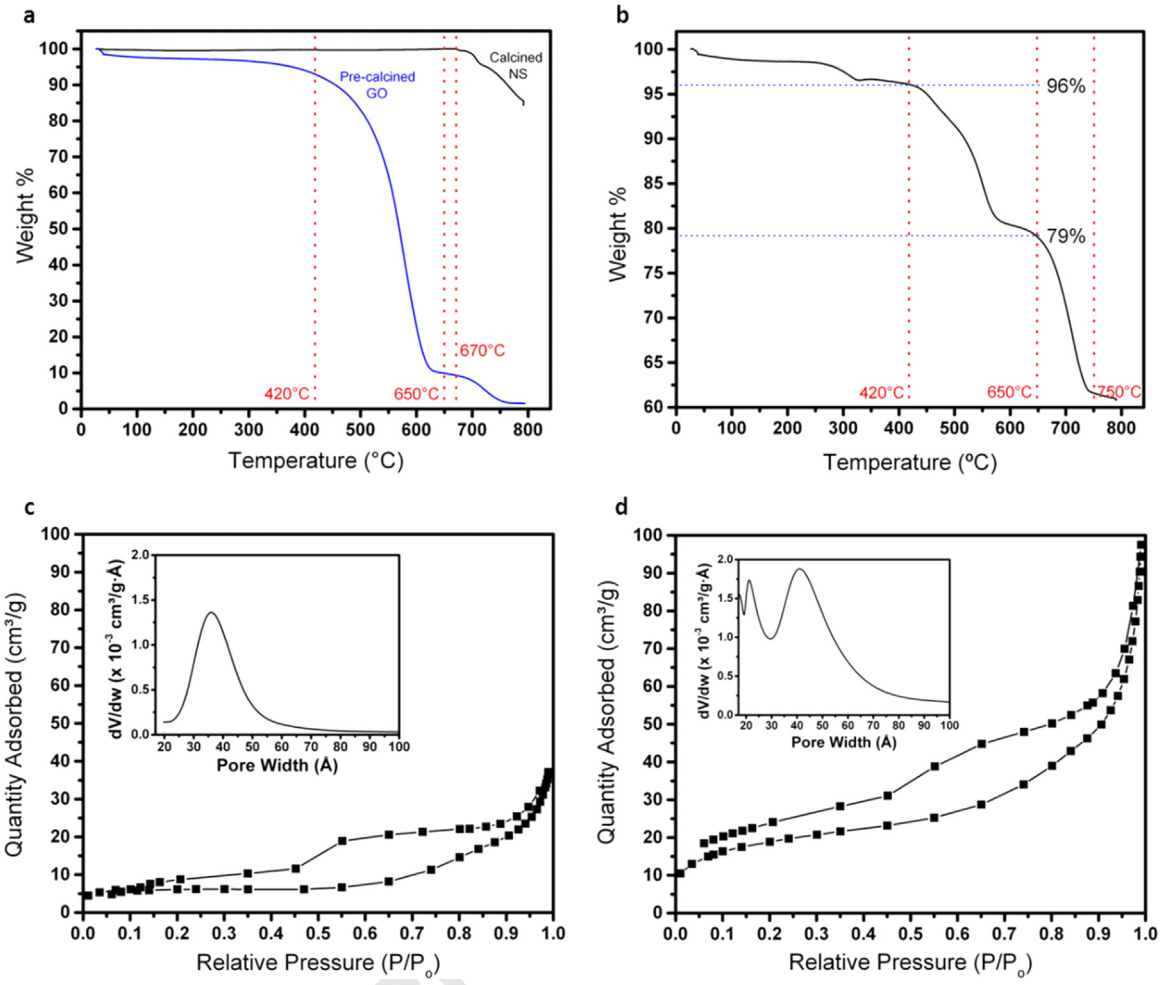

Fig. 6. TGA of (a) pre-calcined GO and calcined NS and (b) calcined NS/G-10. Nitrogen adsorption-desorption isotherms of (c) calcined NS and (d) calcined NS/G-10 (insets: desorption pore size distributions).

in size, causing an increase in the I_D/I_G ratio [37]. The more intense D band could also be attributed to the growth of nickel sulfide nanoprisms on the surface of graphene sheets [18,36].

GO (pre-calcined at 350 °C for 1 h in Ar atmosphere) was analyzed by TGA in air. It was found that the weight loss started at ~420 °C, and over 90% of the weight was lost by ~650 °C (Fig. 6a). Calcined NS showed a weight loss starting at ~670 °C (Fig. 6a). Calcined NS/G-10 exhibited 3 distinct weight loss regions (Fig. 6b). The first of which ended at ~420 °C and was mainly due to loss of moisture and some sulfur [18]. The second region encompassed ~420–650 °C, and the third region was ~650–750 °C. Based on the TGA profiles of the pre-calcined GO and calcined NS, the second and third weight loss regions for calcined NS/G-10 could be associated with graphene and NS, respectively. Thus, the percentage of graphene in calcined NS/G-10 was calculated to be ~17% (from the second weight loss).

Calcined NS and NS/G-10 showed Type IV gas adsorption-desorption isotherms (Fig. 6c and d, respectively), which were characteristic of mesoporous nanocomposites [38]. The Brunauer-Emmett-Teller (BET) specific surface area of calcined NS/G-10 (~66.6 m^2/g) was almost 3 times that of calcined NS (~22.5 m^2/g). Pore size distribution was determined by the Barrett-Joyner-Halenda (BJH) method. Both calcined NS and NS/G-10 were mesoporous in nature; most of the pores were ~4 nm in diameter. However, smaller pores (< 3 nm) were also observed in calcined NS/G-10. The total pore volume of calcined NS/G-10 (~0.15 cm^3/g) was ~3 times that of calcined NS (~0.05 cm^3/g). The higher BET surface area and porosity of calcined NS/G-10 could be attributed to the presence of fine pores of < 3 nm, which would facilitate electrolyte access to electrochemical active sites, and buffer volume change of nickel sulfide during cycling. Such characteristics could enhance the nanocomposite's storage capacity, rate performance and stability during cycling [27].

XPS spectra (0–1300 eV) of calcined NS and NS/G-10 showed peaks at ~162, 285, 532 and 856 eV, which corresponded to S 2p, C 1s, O 1s and Ni 2p, respectively (Fig. 7a and d). The C 1s peak dramatically increased from ~25% in calcined NS to ~74% in calcined NS/G-10, due to graphene wrapping. Ni 2p spectrum of calcined NS was fitted to a spin-orbit doublet and a satellite peak at 853.6, 856.2 and 861.6 eV, respectively (Fig. 7b). Ni 2p spectrum of calcined NS/G-10 was deconvoluted to 2 peaks and a satellite peak at 853.5, 855.8 and 861.7 eV, respectively (Fig. 7e). The doublet and satellite peaks could be assigned to Ni^{2+}, Ni^{3+} and Ni^{2+}, respectively [39–41]. The presence of mixed valences for nickel ions could enhance the conductivity of nickel sulfide by allowing hopping of electrons between cations with low activation energy [42]. S 2p spectrum of calcined NS was deconvoluted into a spin-orbit doublet at 162.1 and 163.0 eV, and a satellite peak at 168.4 eV (Fig. 7c). A spin-orbit doublet and a satellite peak were observed at 161.9, 163.2 and 168.5 eV in the S 2p spectrum of calcined NS/G-10 (Fig. 7f). S 2p spin-orbit doublet corresponded to S $2p_{3/2}$ and S $2p_{1/2}$, respectively, and were attributed to metal-sulfur bonds and S^{2-} [40].

The C 1s spectra of GO and calcined NS/G-10 were compared. C 1s spectrum of GO could be deconvoluted to 3 peaks at 285.0, 286.9 and 289.3 eV (Fig. S2a), which could be assigned to C–C or

Please cite this article as: A.A. AbdelHamid, et al., Graphene-wrapped nickel sulfide nanoprisms with improved performance for Li-ion battery anodes and supercapacitors, Nano Energy (2016), http://dx.doi.org/10.1016/j.nanoen.2016.05.046

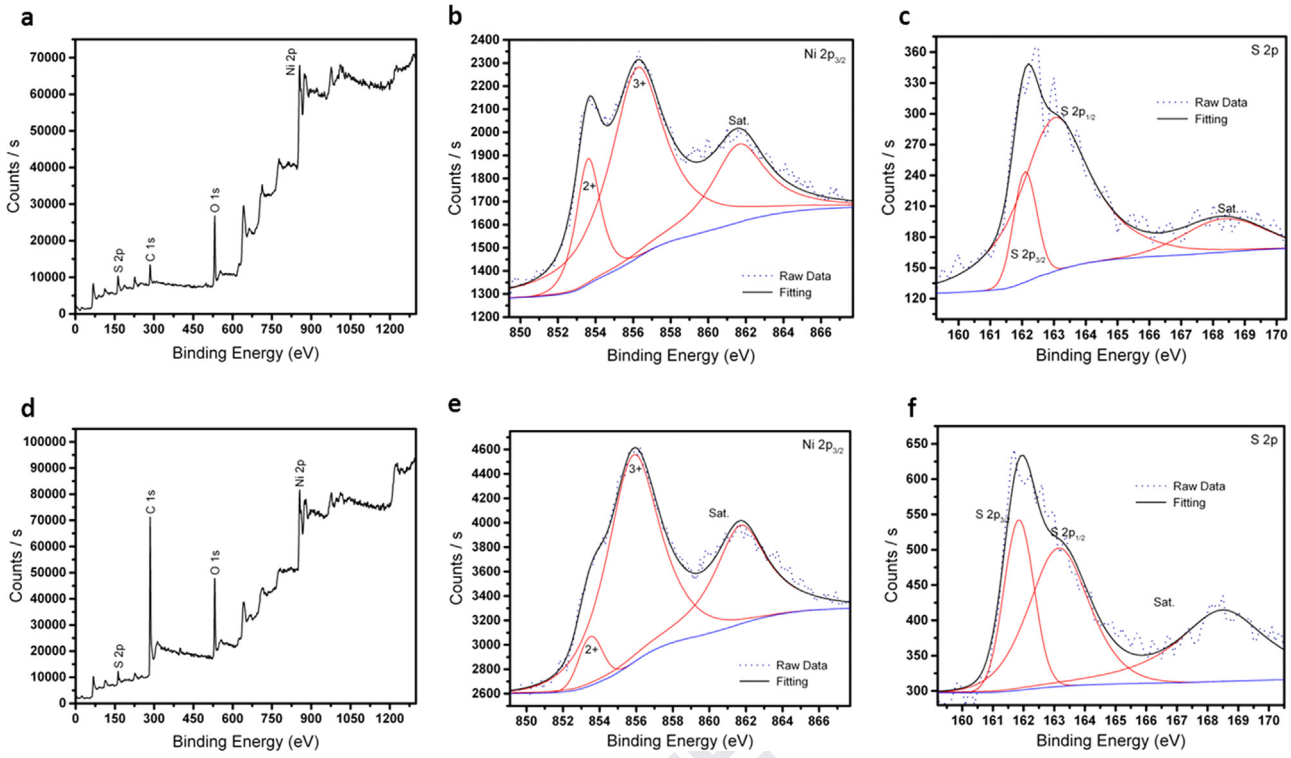

Fig. 7. XPS spectra of (a–c) calcined NS and (d–f) calcined NS/G-10: (a,d) overall, (b,e) Ni $2p_{3/2}$ and (c,f) S 2p spectra.

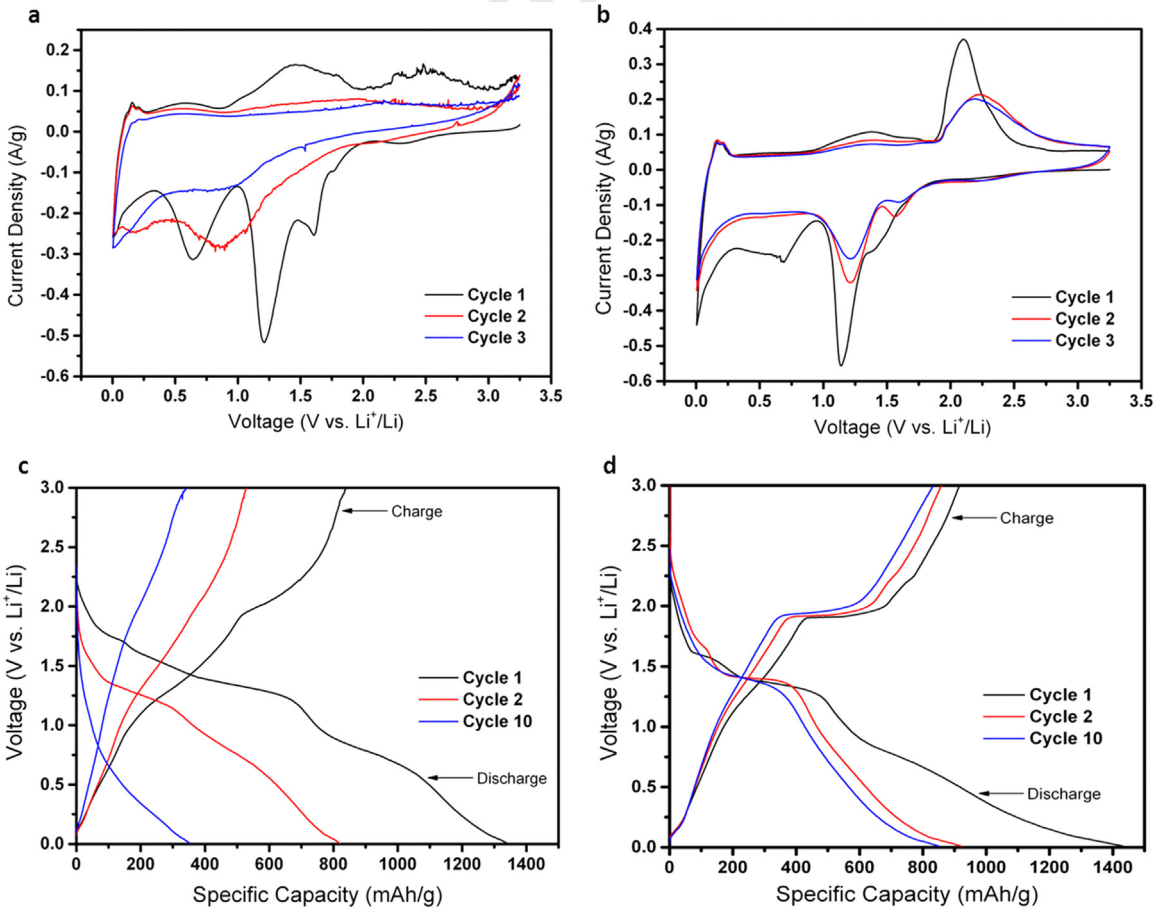

Fig. 8. (a,b) CV curves and (c,d) discharge/charge profiles of calcined (a,c) NS and (b,d) NS/G-10.

Please cite this article as: A.A. AbdelHamid, et al., Graphene-wrapped nickel sulfide nanoprisms with improved performance for Li-ion battery anodes and supercapacitors, Nano Energy (2016), http://dx.doi.org/10.1016/j.nanoen.2016.05.046

C5C, C–O or C5O and –COOH, respectively [43]. C 1s spectrum of calcined NS/G-10 was deconvoluted into 3 peaks at 285.0, 286.0 and 289.1 eV (Fig. S2b). The first peak corresponded to C–C or C5C bonds, while the latter two peaks were attributed to oxygenated species. The intensities of the peaks corresponding to the oxygenated species were decreased in calcined NS/G-10, indicating a decrease in surface oxygenated species from GO.

3.1. Testing as Li-ion battery anode

CV was performed to study the electrochemical behavior of calcined NS and NS/G-10. The first cathodic scan of calcined NS (Fig. 8a) showed a small peak at ~1.6 V and a strong reduction peak at ~1.2 V, which were attributed to the lithium incorporation in Ni_7S_6 (Eq. (2)) [18], and the conversion reaction of Ni_7S_6 to Li_2S and Ni (Eq. (3), respectively.

$$Ni_7S_6 + xLi^+ + xe^- \rightleftharpoons Li_xNi_7S_6 \quad (2)$$

$$Ni_7S_6 + 12Li^+ + 12e^- \rightleftharpoons 7Ni + 6Li_2S \quad (3)$$

Another reduction peak appeared at ~0.65 V, which could be attributed to the formation of solid electrolyte interphase (SEI) due to electrolyte decomposition [14]. In the second cycle, the cathodic peak shifted to ~0.86 V, and was significantly diminished in the third cycle. On the anodic side, the broad peak at ~1.5 V might be due to SEI oxidation [13], while the weak broad peak at ~2.5 V was assigned to the Ni oxidation to nickel sulfide (Eq. (3)). We noted the very low intensity of the Ni oxidation peak, and its disappearance in the subsequent CV cycles of calcined NS.

In contrast, calcined NS/G-10 showed reproducible CV curves with defined reduction and oxidation peaks (Fig. 8b). On the cathodic side, a small broad pre-lithiation peak (Eq. (2)) appeared at ~1.5 V, which shifted in the ~1.6 V in subsequent cycles. The main reduction peak of Ni_7S_6 to Li_2S appeared at ~1.1 V, with no significant shift in subsequent cycles. The peak below 0.7 V could be assigned to the formation of SEI, which was confirmed by its disappearance in the subsequent cycles. On the anodic side, SEI was oxidized at ~1.4 V. Ni oxidation reaction to Ni_7S_6 (Eq. (3)) could be observed at ~2.1 V. In subsequent cycles, the SEI oxidation peak disappeared, and only lithium extraction peak was observed at ~2.2 V.

In the case of calcined NS, the high voltage of Ni oxidation peak compared to calcined NS/G-10 (~2.5 V vs. ~2.1 V) and the significant cathodic peak shift after the first cycle showed electrode polarization. The almost disappearance of the anodic peak and fading of the cathodic peak after the first cycle indicated loss of contact of the active materials due to severe pulverization during reduction and oxidation. On the other hand, the reversible redox peaks of calcined NS/G-10 showed that graphene wrapping helped to maintain the redox reactions of NS nanoprisms, leading to high capacity and cycling stability. This could attributed to the ability of the graphene wrapping to maintain the active materials in good contact with the current collector.

Discharge/charge voltage profiles for calcined NS and NS/G-10 were determined at 70 mA/g, between 0.01 and 3 V (Fig. 8c and d). The first specific discharge capacity of calcined NS was ~1340 mAh/g, while the first specific charge capacity was ~839 mAh/g, with a Coulombic efficiency of ~63%. The very high first discharge capacity and irreversible capacity loss could be due to the decomposition of the electrolyte forming SEI, and the irreversible reactions between NS and Li^+ [13,14]. A small voltage plateau appeared at ~1.7 V corresponding to NS pre-lithiation (Eq. (2), the main plateau was at ~1.3 V corresponding to NS reduction (Eq. (3), and a third plateau at ~0.7 V was attributed to SEI formation. The first charge showed smaller plateaus at ~1.2 V and ~2 V, corresponding to SEI and Ni oxidation, respectively. These discharge and charge plateaus were significantly diminished in the second cycle with a Coulombic efficiency of ~65%, and almost disappeared in the 10th cycle. The disappearance of the discharge and charge voltage plateaus over the first 10 cycles illustrated the poor redox capability and very low capacity retention of bare calcined NS. The low Coulombic efficiencies in the 2nd and 3rd cycles (~65% and ~88%) indicated that a major part of the lithiated active materials could not be de-lithiated. They suggested that reduction caused NS pulverization and contact loss. Coulombic efficiency increased in subsequent cycles reaching ~99% in the 9th cycle, however, discharge capacity had already dropped to ~365 mAh/g.

Calcined NS/G-10's initial discharge and charge capacities were 1432.8 mAh/g and 915.5 mAh/g, respectively, with a Coulombic efficiency of 63.9%. The main voltage plateaus of the first discharge were at ~1.6 V, ~1.3 V and ~0.7 V, corresponding to pre-lithiation, reduction and SEI formation, respectively. The first charge plateau corresponding to Ni oxidation was at ~1.9 V. Discharge capacities in the second and 10th cycles were 922.7 mAh/g and 852.3 mAh/g, respectively, and the charge capacities were 858.7 mAh/g and 833.5 mAh/g, respectively, with Coulombic efficiencies of 93.1% and 97.8%, respectively. The irreversible capacity loss in the first cycle could be attributed to SEI formation. The high Coulombic efficiencies after the first cycle demonstrated the positive effect of graphene on the maintenance of NS redox reactions. The stability of the voltage profiles in the first 10 cycles further confirmed that the nanocomposite underwent stable lithium insertion and extraction, and that graphene wrapping of NS nanoprisms stabilized the redox process by providing a conductive support that can maintain the engagement of the active materials in the redox processes.

Cyclic performance of calcined NS/G-10 was assessed at 70 mA/g between 0.01 V and 3 V (Fig. 9a). NS/G-10 suffered an irreversible capacity loss in the first cycle due to SEI formation, and capacity fading continued for 6 cycles. However, this trend was reversed, and the capacity increased until the 100th cycle, reaching ~1220 mAh/g. Capacity increase over cycling was previously reported for CoO, and was explained by the slow reaction of irreversible Li_2O that was formed during the first discharge [44]. Another possible mechanism was the disintegration of the NS nanoparticles over cycling, which increased the surface area of the exposed active material, resulting in enhanced capacity. This could be inferred from the TEM images of calcined NS/G-10 after 3 and 30 cycles (Fig. S3a and b). After 3 cycles, the nanoprisms were still observed on the surface of graphene sheets, while after 30 cycles, irregular and very small particles were observed instead. The presence of graphene helped to maintain the active material's engagement after its disintegration. It also mitigated polysulfide dissolution and enhanced electron and ionic transport [18,27]. After 100 cycles, the capacity started to decay, reaching ~622 mAh/g after 200 cycles. This might be due to the end of the activation period and the slow contact loss of the active material. It could also be due to other metal sulfide capacity decay mechanisms, such as polysulfide dissolution. A high Coulombic efficiency of $\geq$96% was maintained during the 200 cycles. On the other hand, calcined NS did not show any activation period, and its capacity decreased dramatically during the first 20 cycles, reaching ~236 mAh/g after 50 cycles (Fig. 9b). The absence of the activation period in calcined NS is due to the contact loss with the current collector, which isolated the active material and prevented any capacity increase.

GO content was varied during the synthesis of NS/G, in order to determine the effect of graphene loading on the nanocomposite's electrochemical performance. Calcined NS/G-5 and NS/G-20 were analyzed using TGA to determine their graphene contents. The

Please cite this article as: A.A. AbdelHamid, et al., Graphene-wrapped nickel sulfide nanoprisms with improved performance for Li-ion battery anodes and supercapacitors, Nano Energy (2016), http://dx.doi.org/10.1016/j.nanoen.2016.05.046

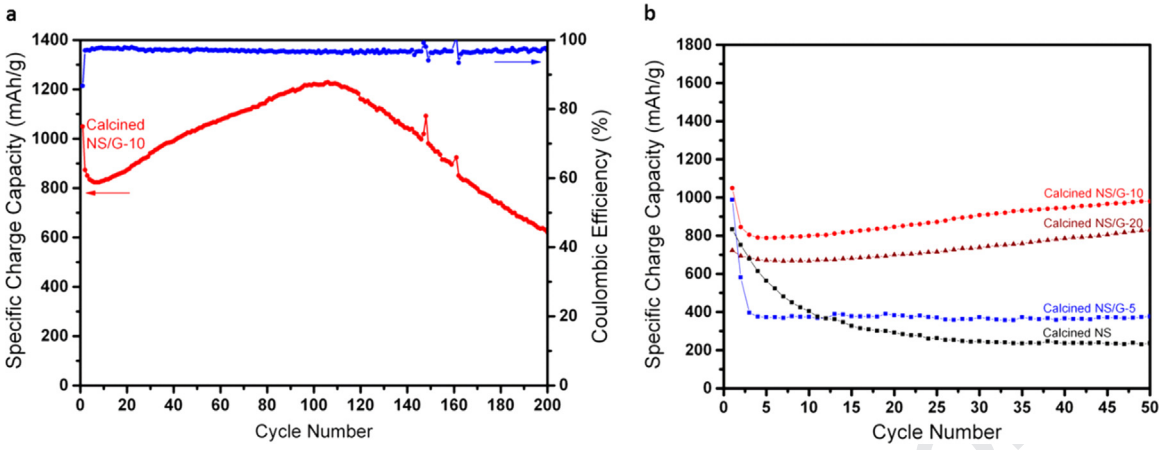

Fig. 9. (a) Cycling performance and Coulombic efficiency of calcined NS/G-10. (b) Cycling performance of calcined NS, NS/G-5, NS/G-10 and NS/G-20.

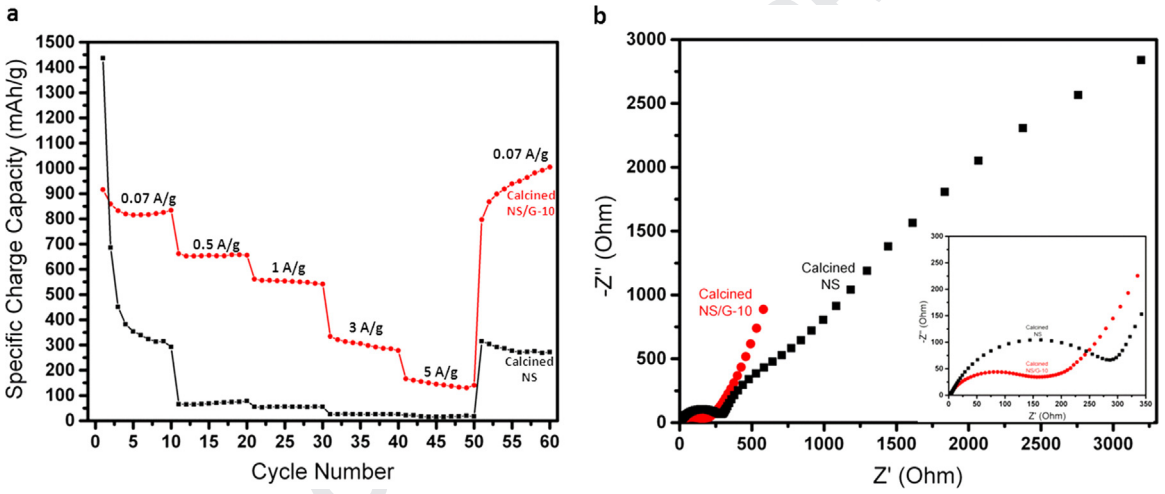

Fig. 10. (a) Rate performance and (b) EIS of calcined NS and NS/G-10.

loading of graphene in calcined NS/G-5 and NS/G-20 was ~8.5 wt% and ~30 wt%, respectively (Fig. S4). Cycling stability of calcined NS/G-5 was very poor as compared to NS/G-10; NS/G-5's capacity decreased to ~380 mAh/g after 50 cycles (Fig. 9b). Although it exceeded calcined NS in specific capacity by ~140 mAh/g, the rapid decrease in capacity showed that the amount of graphene in the nanocomposite was not sufficient to stabilize nickel sulfide and maintain its redox processes. NS/G-20's specific capacity reached ~830 mAh/g after 50 cycles (Fig. 9b), which was superior to the performance of calcined NS and NS/G-5. However, it was still lower than that of NS/G-10, which was ~980 mAh/g after 50 cycles. Although the loading of graphene in NS/G-20 was almost double that in NS/G-10, its specific capacity was lower. These results indicated that the optimum amount of graphene for stabilizing the electrochemical performance in the nanocomposite was ~10–20%. Nanocomposites containing higher loading of graphene still have good performance, but they have lower specific capacities due to a lower loading of nickel sulfide in the nanocomposite, which decreased the theoretical capacity.

Calcined NS and NS/G-10 were cycled at higher current densities in order to assess their rate performance (Fig. 10a). Calcined NS/G-10 showed specific charge capacities of ~834, 656, 542, 278 and 141 mAh/g at the 10th cycle at current densities of 0.07, 0.5, 1, 3 and 5 A/g, respectively. It also displayed excellent ability to recover when it was charged again at 0.07 A/g, whereby it achieved a specific charge capacity of ~1005 mAh/g at the 10th cycle. In contrast, calcined NS showed specific charge capacities of ~292, 78, 55, 26 and 17 mAh/g at 0.07, 0.5, 1, 3 and 5 A/g, respectively, at the 10th cycle. After recharging at 0.07 A/g, ~272 mAh/g was recovered at the 10th cycle. The superior rate performance of NS/G-10 was attributed to the ability of graphene to maintain good dispersion of the NS nanoprisms, which shortened electron and Li^+ diffusion paths and enhanced the electrode kinetics. In addition, the larger specific surface area and pore volume of the nanocomposite allowed for greater electrolyte access to the electrochemically active sites, which further improved electrode kinetics. Moreover, graphene wrapping formed a conductive network that boosted the electrode conductivity, improving the rate performance.

Nyquist plots (Fig. 10b) showed that the diameter of the semicircle in the medium-frequency region was reduced upon incorporation of graphene (Fig. 10b inset), indicating a lower contact and charge transfer impedance compared to calcined NS [18]. This was attributed to the conductive network formed by graphene, which wrapped around the NS nanoprisms. The higher slope of the inclined line in the low frequency region of calcined NS/G-10's plot showed a lower Warburg impedance. This indicated that the Li^+ diffusion was facilitated in the nanocomposite [18,45]. It could be due to less aggregation of NS nanoprisms, and the higher specific surface area and pore volume of the nanocomposite.

Full cell was assembled in order to test the performance of calcined NS/G-10 for practical applications. Full cells are more

Please cite this article as: A.A. AbdelHamid, et al., Graphene-wrapped nickel sulfide nanoprisms with improved performance for Li-ion battery anodes and supercapacitors, Nano Energy (2016), http://dx.doi.org/10.1016/j.nanoen.2016.05.046

challenging due to the absence Li metal anode, which acts as an abundant Li ion source and a stable reference electrode [46]. The full cell was cycled at a current of 70 mA/g (for calcined NS/G-10). Fig. S5a shows the first charge/discharge voltage profile, where the specific capacity of the full cell at the first charge was ~146 mAh/g, while that of the first discharge was ~104 mAh/g, with a Coulombic efficiency of ~71%. The specific capacity decreased to ~80.3 mAh/g after 9 cycles (Fig. S5b).

High-voltage anodes are needed to avoid the safety concerns that are associated with graphite [47]. Lithium titanate (1.5 V vs. Li^+/Li) [47] has been used as a high-voltage anode in full cell with $LiFePO_4$ as cathode [48,49]. Although metal sulfides [13,14,17,50] have higher voltages (de-lithiation at $\geq$2 V vs. Li^+/Li) than typical high-voltage anodes, they have much higher specific capacity. This can lead to comparable or even higher full-cell energy density [51]. Thus, graphene-wrapped nickel sulfide nanoprisms, having high operating voltage (de-lithiation at ~1.9 V vs. Li^+/Li), can be used as a high-voltage anode.

Graphene wrapping was used to avoid the substantial capacity loss shown by bare nickel sulfide nanoprisms, achieving high specific capacity over the first 100 cycles. However, graphene-wrapped nickel sulfide began to decrease in capacity in subsequent cycles, probably caused by slow detachment of the disintegrated active material from the surface of graphene sheets. To reduce material detachment and improve stability, the nanocomposite would need to be further improved, for example by increasing the graphene content or by embedding the nickel sulfide nanoprisms within a carbon matrix. The full-cell configuration should also be further optimized for capacity and stability in practical applications.

3.2. Testing as supercapacitor electrode

CV curves of calcined NS and NS/G-10 showed redox peaks characteristic of pseudocapacitors (Fig. 11a and b). This was different from the rectangular CV curves that are shown by electric double layer supercapacitors [25]. The symmetrical redox peaks indicated good reversibility of the redox reactions [23]. At high scan rates, the anodic and cathodic peaks shifted to higher and lower voltages, respectively, due to electrode polarization at high current densities [22]. It was observed that the linear relationship between the cathodic peak current (i_p) and the scan rate (V) could be best fitted as i_p vs. $V^{1/2}$ (Fig. S6a and b). This showed that the redox reaction of nickel sulfide was diffusion limited [24].

Based on previous reports [22,24], the redox peaks observed in the CV curves could be assigned to the following reaction:

$$Ni_{1.17}S + OH^- \rightleftharpoons Ni_{1.17}SOH + e^- \quad (4)$$

According to the previous equation, the theoretical specific capacitance was calculated to be ~2130 F/g using the following equation [40],

$$C_s = Q/\Delta V = nF/m\Delta V \quad (5)$$

where C_s is the theoretical specific capacitance, Q is the amount of charge stored per gram of active material, ΔV is the potential window, n is the number of charge transferred during the redox reactions, F is Faraday constant and m is the molar mass of the active material.

Chronopotentiometry was conducted at current densities of 3–20 A/g in a potential window of 0–0.45 V vs. Ag/AgCl (Fig. 11c and d). The potential plateaus during charge and discharge

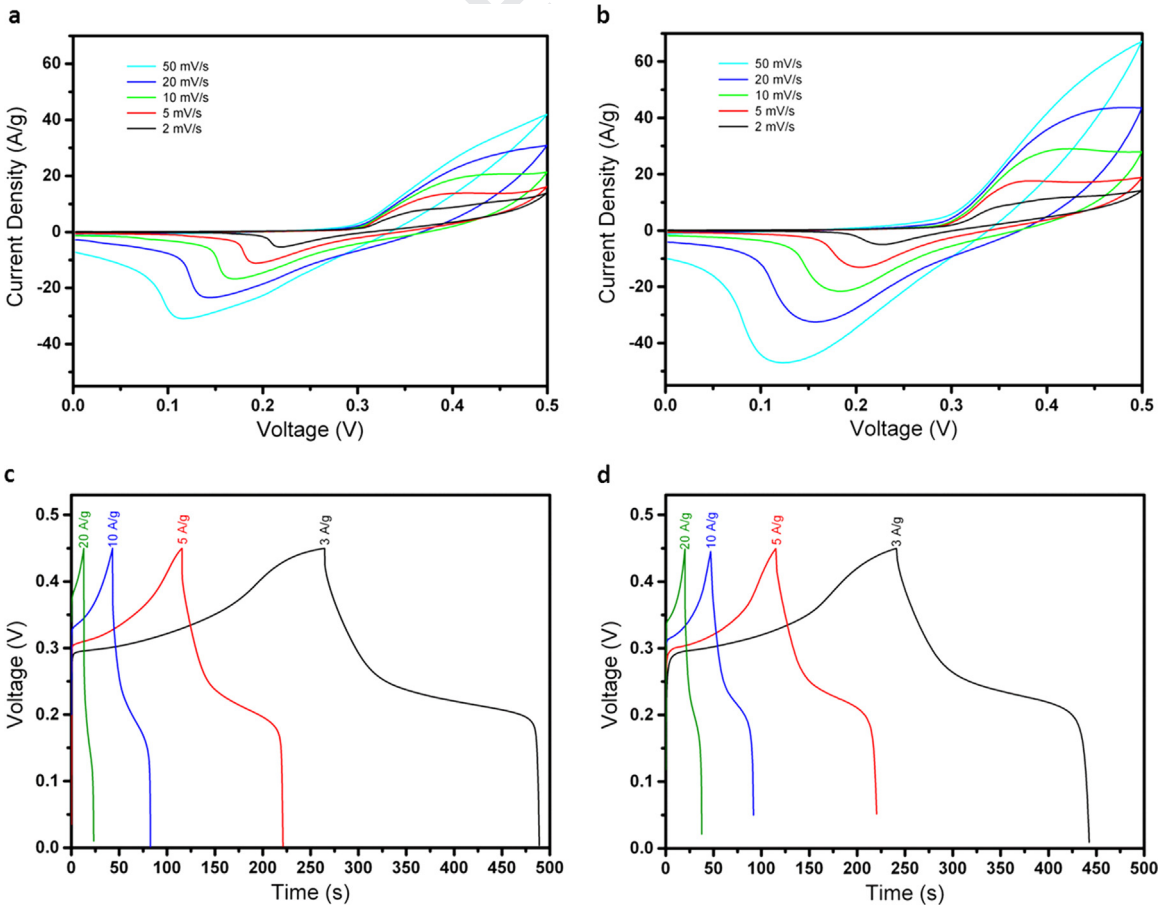

Fig. 11. (a,b) CV curves of calcined (a) NS and (b) NS/G-10. (c, d) Chronopotentiometry curves of calcined (c) NS and (d) NS/G-10 at various current densities.

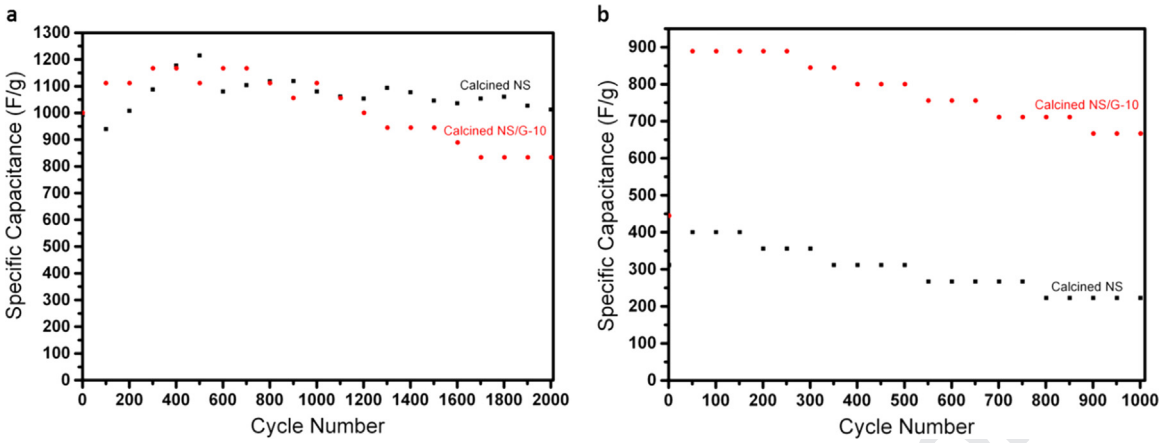

Fig. 12. Cycling performance of calcined NS and NS/G-10 at a current density of (a) 5 A/g and (b) 20 A/g.

corresponded to the CV oxidation and reduction peaks, respectively. The symmetrical charge and discharge curves indicated good pseudocapacitive properties and reversible redox reactions [24]. Calcined NS achieved specific capacitances of ~1495, 1171, 878 and 449 F/g at 3, 5, 10 and 20 A/g, respectively (Fig. S7). Calcined NS/G-10 achieved specific capacitances of ~1337, 1156, 956 and 777.8 F/g at 3, 5, 10 and 20 A/g, respectively (Fig. S7). It was observed that calcined NS/G-10 showed better performance at high current densities (10 and 20 A/g). At 20 A/g, calcined NS retained only 30% of the specific capacitance achieved at 3 A/g, while calcined NS/G-10 could retain ~58%. This showed that the nanocomposite improved the redox behavior of nickel sulfide at high current densities.

Cyclic performance was evaluated by continuous charge and discharge for 2000 cycles at 5 A/g, in the potential range of 0–0.45 V vs. Ag/AgCl (Fig. 12a). The specific capacitance of calcined NS increased over the first 500 cycles until ~1210 F/g. It was relatively stable at 1000–1100 F/g over the next 1500 cycles. The specific capacitance after 2000 cycles was ~1010 F/g, which is ~83% of the maximum specific capacitance. Similarly, the specific capacitance of calcined NS/G-10 increased over the first 300 cycles to ~1170 F/g. It slightly decreased to ~1110 F/g after 1000 cycles, and then gradually declined to about 830 F/g after 2000 cycles. It could retain ~71% of its maximum specific capacitance after 2000 cycles.

The presence of graphene did not improve the cycling performance of nickel sulfide. The NS/G-10 nanocomposite actually showed a lower specific capacitance after 2000 cycles. However, the cycling performance at 20 A/g was different. Calcined NS and NS/G-10 achieved maximum specific capacitances of ~400 and 890 F/g, respectively after 100 cycles (Fig. 12b). The specific capacitances then decreased gradually reaching ~220 and 670 F/g, respectively after 1000 cycles. The 3-fold higher specific capacitance of calcined NS/G-10 compared to calcined NS after 1000 cycles showed that graphene had a critical role in improving the pseudocapacitive performance of nickel sulfide at high current densities.

The specific capacitance of calcined NS at a current density of 5 A/g was compared to previous reports of nickel sulfide at the same or lower current densities. Our calcined NS had higher specific capacitance than Ni_3S_2 [24], NiS [22,26,52,53], NiS_2 [23] and mixed-phase nickel sulfides [20,54,55]. The performance of the nickel sulfide nanoprisms could be attributed to their small size, which shortened the ionic and electronic diffusion paths [6], exposed more electroactive sites, and improved contact with the electrolyte [8]. Carbon coating upon calcination might have contributed to the high pseudocapacitive performance by improving electronic transport [56] and stabilizing the nanoparticles. The single-crystalline nanoprismatic structure could have facilitated diffusion of electrons and improved the electrochemical activity, as previously reported for NiS_2 nanocubes [23].

Graphene wrapping of the nickel sulfide nanoprisms did not improve their pseudocapacitive properties at low current densities. However, graphene's presence was important at high current densities. This could be explained by the enhanced electronic transport due to the high conductivity of graphene, which improved the electrode kinetics [54]. This was augmented by the direct anchoring of the nanoprisms on the surface of the graphene sheets, which further facilitated electronic transport [36]. In addition, the higher surface area and porosity of the nanocomposite facilitated electrolyte transport and ionic diffusion, which improved the rate capability of the electrode [25,54].

4. Conclusions

Nickel sulfide nanoprisms were prepared by a facile synthesis method. They had high initial specific capacity when used as Li-ion battery anode, but suffered from rapid capacity fading. As supercapacitor electrode, they demonstrated remarkable specific capacitances of ~1495 and 1171 F/g at current densities of 3 and 5 A/g, respectively. Graphene wrapping was used to improve the electrochemical properties of nickel sulfide nanoprisms. It dramatically improved the performance of the Li-ion battery anode material, achieving a specific capacity of over 1200 mAh/g after 100 cycles. Graphene also helped to improve the pseudocapacitive rate performance, enabling the nanocomposite to achieve a 3-fold higher specific capacitance at 20 A/g after 1000 cycles.

Acknowledgements

This work was funded by the Institute of Bioengineering and Nanotechnology (Biomedical Research Council, Agency for Science, Technology and Research, Singapore).

Appendix A. Supplementary material

Supplementary data associated with this article can be found in the online version at http://dx.doi.org/10.1016/j.nanoen.2016.05.046.

Please cite this article as: A.A. AbdelHamid, et al., Graphene-wrapped nickel sulfide nanoprisms with improved performance for Li-ion battery anodes and supercapacitors, Nano Energy (2016), http://dx.doi.org/10.1016/j.nanoen.2016.05.046

References

[1] B. Scrosati, J. Garche, J. Power Sources 195 (2010) 2419–2430.
[2] R. Marom, S.F. Amalraj, N. Leifer, D. Jacob, D. Aurbach, J. Mater. Chem. 21 (2011) 9938.
[3] P. Poizot, S. Laruelle, S. Grugeon, L. Dupont, J.M. Tarascon, Nature 407 (2000) 496–499.
[4] P.G. Bruce, B. Scrosati, J.-M. Tarascon, Angew. Chem. Int. Ed. 47 (2008) 2930–2946.
[5] C. Jiang, E. Hosono, H. Zhou, Nano Today 1 (2006) 28–33.
[6] C.-C. Hu, K.-H. Chang, M.-C. Lin, Y.-T. Wu, Nano Lett. 6 (2006) 2690–2695.
[7] W. Xiao, H. Xia, J.Y.H. Fuh, L. Lu, J. Power Sources 193 (2009) 935–938.
[8] Z. Jiang, W. Lu, Z. Li, K.H. Ho, X. Li, X. Jiao, D. Chen, J. Mater. Chem. A 2 (2014) 8603.
[9] L. Zhang, L. Zhou, H.B. Wu, R. Xu, X.W. Lou, Angew. Chem. Int. Ed. 51 (2012) 7267–7270.
[10] Y. Wang, Q. Zhu, L. Tao, X. Su, J. Mater. Chem. 21 (2011) 9248.
[11] Q. Wang, R. Gao, J. Li, Appl. Phys. Lett. 90 (2007) 143107.
[12] P. Poizot, S. Laruelle, S. Grugeon, J.-M. Tarascon, J. Electrochem. Soc. 149 (2002) A1212–A1217.
[13] W. Shi, J. Zhu, X. Rui, X. Cao, C. Chen, H. Zhang, H.H. Hng, Q. Yan, ACS Appl. Mater. Interfaces 4 (2012) 2999–3006.
[14] C. Xu, Y. Zeng, X. Rui, N. Xiao, J. Zhu, W. Zhang, J. Chen, W. Liu, H. Tan, H.H. Hng, Q. Yan, ACS Nano 6 (2012) 4713–4721.
[15] X. Zhu, Z. Wen, Z. Gu, S. Huang, J. Electrochem. Soc. 153 (2006) A504–A507.
[16] N.H. Idris, M.M. Rahman, S.-L. Chou, J.-Z. Wang, D. Wexler, H.-K. Liu, Electrochim. Acta 58 (2011) 456–462.
[17] M.Y. Son, J.H. Choi, Y.C. Kang, J. Power Sources 251 (2014) 480–487.
[18] N. Mahmood, C. Zhang, Y. Hou, Small 9 (2013) 1321–1328.
[19] H. Wan, X. Ji, J. Jiang, J. Yu, L. Miao, L. Zhang, S. Bie, H. Chen, Y. Ruan, J. Power Sources 243 (2013) 396–402.
[20] W. Wei, L. Mi, Y. Gao, Z. Zheng, W. Chen, X. Guan, Chem. Mater. 26 (2014) 3418–3426.
[21] Q. Wang, L. Jiao, H. Du, J. Yang, Q. Huan, W. Peng, Y. Si, Y. Wang, H. Yuan, CrystEngComm 13 (2011) 6960.
[22] B.T. Zhu, Z. Wang, S. Ding, J.S. Chen, X.W. Lou, RSC Adv. 1 (2011) 397.
[23] H. Pang, C. Wei, X. Li, G. Li, Y. Ma, S. Li, J. Chen, J. Zhang, Sci. Rep. 4 (2014).
[24] S.-W. Chou, J.-Y. Lin, J. Electrochem. Soc. 160 (2013) D178–D182.
[25] J. Yang, X. Duan, W. Guo, D. Li, H. Zhang, W. Zheng, Nano Energy 5 (2014) 74–81.
[26] A. Wang, H. Wang, S. Zhang, C. Mao, J. Song, H. Niu, B. Jin, Y. Tian, Appl. Surf. Sci. 282 (2013) 704–708.
[27] G. Zhou, D.-W. Wang, F. Li, L. Zhang, N. Li, Z.-S. Wu, L. Wen, G.Q. Lu, H.-M. Cheng, Chem. Mater. 22 (2010) 5306–5313.
[28] J. Song, Z. Yu, M.L. Gordin, S. Hu, R. Yi, D. Tang, T. Walter, M. Regula, D. Choi, X. Li, A. Manivannan, D. Wang, Nano Lett. 14 (2014) 6329–6335.
[29] S. Evers, L.F. Nazar, Chem. Commun. 48 (2012) 1233–1235.
[30] X.-F. Yang, J.-H. Yang, Y.L. Zhong, V. Gariepy, M.L. Trudeau, K. Zaghib, J.Y. Ying, ChemSusChem 7 (2014) 1618–1622.
[31] A. Ghezelbash, M.B. Sigman, B.A. Korgel, Nano Lett. 4 (2004) 537–542.
[32] A. Ghezelbash, B.A. Korgel, Langmuir 21 (2005) 9451–9456.
[33] A.L. Abdelhady, M.A. Malik, P. O'Brien, F. Tuna, J. Phys. Chem. C 116 (2011) 2253–2259.
[34] T. Zhang, P. Liu, C. Sheng, Y. Duan, J. Zhang, Chem. Commun. 50 (2014) 2889–2892.
[35] P. Parreira, G. Lavareda, A. Amaral, A.M. Botelho do Rego, O. Conde, J. Valente, F. Nunes, C. Nunes de Carvalho, J. Alloy. Compd. 509 (2011) 5099–5104.
[36] H. Zhang, X. Yu, D. Guo, B. Qu, M. Zhang, Q. Li, T. Wang, ACS Appl. Mater. Interfaces 5 (2013) 7335–7340.
[37] S. Stankovich, D.A. Dikin, R.D. Piner, K.A. Kohlhaas, A. Kleinhammes, Y. Jia, Y. Wu, S.T. Nguyen, R.S. Ruoff, Carbon 45 (2007) 1558–1565.
[38] M. Kruk, M. Jaroniec, Chem. Mater. 13 (2001) 3169–3183.
[39] Q. Liu, J. Jin, J. Zhang, ACS Appl. Mater. Interfaces 5 (2013) 5002–5008.
[40] J. Pu, T. Wang, H. Wang, Y. Tong, C. Lu, W. Kong, Z. Wang, ChemPlusChem 79 (2014) 577–583.
[41] J. Pu, F. Cui, S. Chu, T. Wang, E. Sheng, Z. Wang, ACS Sustain. Chem. Eng. 2 (2013) 809–815.
[42] M. Hamdani, R.N. Singh, P. Chartier, Int. J. Electrochem. Sci. 5 (2010) 556–577.
[43] Y. Feng, N. Feng, G. Zhang, G. Du, CrystEngComm 16 (2014) 214–222.
[44] J.-S. Do, C.-H. Weng, J. Power Sources 146 (2005) 482–486.
[45] J. Liu, C. Liu, Y. Wan, W. Liu, Z. Ma, S. Ji, J. Wang, Y. Zhou, P. Hodgson, Y. Li, CrystEngComm 15 (2013) 1578.
[46] X.L. Wang, W.Q. Han, H. Chen, J. Bai, T.A. Tyson, X.Q. Yu, X.J. Wang, X.Q. Yang, J. Am. Chem. Soc. 133 (2011) 20692–20695.
[47] Y. Yang, B. Qiao, X. Yang, L. Fang, C. Pan, W. Song, H. Hou, X. Ji, Adv. Funct. Mater. 24 (2014) 4349–4356.
[48] A. Jaiswal, C.R. Horne, O. Chang, W. Zhang, W. Kong, E. Wang, T. Chern, M. M. Doeff, J. Electrochem. Soc. 156 (2009) A1041.
[49] Y. Liu, S. Gorgutsa, C. Santato, M. Skorobogatiy, J. Electrochem. Soc. 159 (2012) A349.
[50] H. Hwang, H. Kim, J. Cho, Nano Lett. 11 (2011) 4826–4830.
[51] X. Xu, S. Jeong, C.S. Rout, P. Oh, M. Ko, H. Kim, M.G. Kim, R. Cao, H.S. Shin, J. Cho, J. Mater. Chem. A 2 (2014) 10847–10853.
[52] J. Yang, W. Guo, D. Li, C. Wei, H. Fan, L. Wu, W. Zheng, J. Power Sources 268 (2014) 113–120.
[53] X. Yan, X. Tong, L. Ma, Y. Tian, Y. Cai, C. Gong, M. Zhang, L. Liang, Mater. Lett. 124 (2014) 133–136.
[54] Z. Xing, Q. Chu, X. Ren, J. Tian, A.M. Asiri, K.A. Alamry, A.O. Al-Youbi, X. Sun, Electrochem. Commun. 32 (2013) 9–13.
[55] X. Liu, X. Qi, Z. Zhang, L. Ren, Y. Liu, L. Meng, K. Huang, J. Zhong, Ceram. Int. 40 (2014) 8189–8193.
[56] X.-F. Zhang, K.-X. Wang, X. Wei, J.-S. Chen, Chem. Mater. 23 (2011) 5290–5292.

Ayman A. AbdelHamid received his M.Sc. in nanotechnology from Nile University, Egypt in 2012. He is currently a Ph.D. student at Nanyang Technological University, Singapore. He conducts his thesis research on energy storage nanocomposite materials at the Institute of Bioengineering and Nanotechnology (IBN) as a SINGA scholar.

Xianfeng Yang received his Ph.D. from Sun Yat-Sen University in 2008, where he also spent two years as a Postdoctoral Research Fellow. He was a Research Associate with Prof. Jimmy C. Yu at the Chinese University of Hong Kong in 2008–2009. He was a Research Scientist in Prof. Jackie Y. Ying's group at IBN in Singapore during 2010–2014. He is now a professor at South China University of Technology. His research interests include the development of nanomaterials for energy-related applications, and the relationship between microstructure and properties.

Jinhua Yang received his Ph.D. in Chemical and Bimolecular Engineering from National University of Singapore in 2010. He is a Research Scientist at IBN. His research is focused on the synthesis and characterization of inorganic materials for electrochemical applications in fuel cells, batteries and supercapacitors.

Xiaojun Chen graduated from Harbin Institute of Technology with B.S. in applied electrochemistry, and Zhejiang University with M.S. in chemical engineering. He received his Ph.D. from Nanyang Technological University in materials science. He has over 10 years of R&D and project management experience. His research is focused on electrochemistry, biosensors, fuel cells and lithium-ion batteries. He has published over 40 peer-reviewed papers in refereed journals.

Jackie Y. Ying received her B.E. and Ph.D. from The Cooper Union and Princeton University, respectively. She joined the faculty at Massachusetts Institute of Technology in 1992, where she was Professor of Chemical Engineering until 2005. She has been the Founding Executive Director of the Institute of Bioengineering and Nanotechnology in Singapore since 2003. For her research on nanostructured materials, Prof. Ying has been recognized with the American Ceramic Society Ross C. Purdy Award, David and Lucile Packard Fellowship, Office of Naval Research Young Investigator Award, National Science Foundation Young Investigator

Please cite this article as: A.A. AbdelHamid, et al., Graphene-wrapped nickel sulfide nanoprisms with improved performance for Li-ion battery anodes and supercapacitors, Nano Energy (2016), http://dx.doi.org/10.1016/j.nanoen.2016.05.046

Award, Camille Dreyfus Teacher-Scholar Award, American Chemical Society Faculty Fellowship Award in Solid-State Chemistry, Technology Review's Inaugural TR100 Young Innovator Award, American Institute of Chemical Engineers (AIChE) Allan P. Colburn Award, Singapore National Institute of Chemistry-BASF Award in Materials Chemistry, Wall Street Journal Asia's Asian Innovation Silver Award, International Union of Biochemistry and Molecular Biology Jubilee Medal, Materials Research Society Fellowship, Royal Society of Chemistry Fellowship, Crown Prince Grand Prize in the Brunei Creative, Innovative Product and Technological Advancement (CIPTA) Award, American Institute for Medical and Biological Engineering Fellowship, Academy of Sciences of Iran Medal of Honor, American Association for the Advancement of Science Fellowship, Singapore National Academy of Science Fellowship, and The Cooper Union Alumni Association Gano Dunn Award. Prof. Ying was elected a World Economic Forum Young Global Leader, and a member of the German National Academy of Sciences, Leopoldina. She was named one of the "One Hundred Engineers of the Modern Era" by AIChE in its Centennial Celebration. She was selected as an Inaugural Inductee for the Singapore Women's Hall of Fame in 2014. She was the inaugural winner of the Mustafa Prize "Top Scientific Achievement Award" in 2015 for her research in bio-nanotechnology. She is the Editor-in-Chief of *Nano Today*.

Please cite this article as: A.A. AbdelHamid, et al., Graphene-wrapped nickel sulfide nanoprisms with improved performance for Li-ion battery anodes and supercapacitors, Nano Energy (2016), http://dx.doi.org/10.1016/j.nanoen.2016.05.046